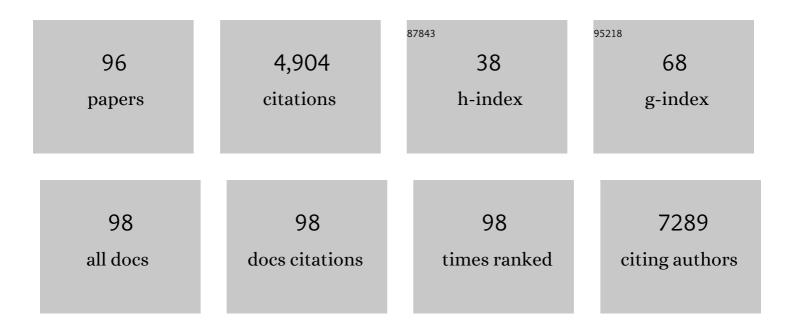


List of Publications by Year in descending order

Source: https://exaly.com/author-pdf/1830851/publications.pdf Version: 2024-02-01



Μιλο Υμ

#	Article	IF	CITATIONS
1	One-step production of O-N-S co-doped three-dimensional hierarchical porous carbons for high-performance supercapacitors. Nano Energy, 2018, 47, 547-555.	8.2	547
2	Three-dimensional scaffolding framework of porous carbon nanosheets derived from plant wastes for high-performance supercapacitors. Nano Energy, 2016, 27, 377-389.	8.2	391
3	True Nature of an Archetypal Self-Assembly System: Mobile Au-Thiolate Species on Au(111). Physical Review Letters, 2006, 97, 166102.	2.9	239
4	Multifunctional Bismuth Selenide Nanocomposites for Antitumor Thermo-Chemotherapy and Imaging. ACS Nano, 2016, 10, 984-997.	7.3	234
5	Multimodal Imaging-Guided Antitumor Photothermal Therapy and Drug Delivery Using Bismuth Selenide Spherical Sponge. ACS Nano, 2016, 10, 9646-9658.	7.3	175
6	Sulphur-doped carbon nanosheets derived from biomass as high-performance anode materials for sodium-ion batteries. Nano Energy, 2020, 67, 104219.	8.2	143
7	iASPP Is an Antioxidative Factor and Drives Cancer Growth and Drug Resistance by Competing with Nrf2 for Keap1 Binding. Cancer Cell, 2017, 32, 561-573.e6.	7.7	130
8	Dual-Stimuli Responsive Bismuth Nanoraspberries for Multimodal Imaging and Combined Cancer Therapy. Nano Letters, 2018, 18, 6778-6788.	4.5	116
9	Phaseâ€Transition Induced Conversion into a Photothermal Material: Quasiâ€Metallic WO _{2.9} Nanorods for Solar Water Evaporation and Anticancer Photothermal Therapy. Angewandte Chemie - International Edition, 2018, 57, 10666-10671.	7.2	104
10	Carbon dots-fed Shewanella oneidensis MR-1 for bioelectricity enhancement. Nature Communications, 2020, 11, 1379.	5.8	97
11	Dual-phase molybdenum nitride nanorambutans for solar steam generation under one sun illumination. Nano Energy, 2019, 57, 842-850.	8.2	96
12	Highly porous PEGylated Bi ₂ S ₃ nano-urchins as a versatile platform for in vivo triple-modal imaging, photothermal therapy and drug delivery. Nanoscale, 2016, 8, 16005-16016.	2.8	90
13	Biowaste-Derived Hierarchical Porous Carbon Nanosheets for Ultrahigh Power Density Supercapacitors. ChemSusChem, 2018, 11, 1678-1685.	3.6	90
14	One-pot green synthesis of bimetallic hollow palladium-platinum nanotubes for enhanced catalytic reduction of p-nitrophenol. Journal of Colloid and Interface Science, 2019, 539, 161-167.	5.0	90
15	Photothermal conversion-coordinated Fenton-like and photocatalytic reactions of Cu2-xSe-Au Janus nanoparticles for tri-combination antitumor therapy. Biomaterials, 2020, 255, 120167.	5.7	89
16	A solution to break the salt barrier for high-rate sustainable solar desalination. Energy and Environmental Science, 2021, 14, 2451-2459.	15.6	87
17	Ti-modified hierarchical mordenite as highly active catalyst for oxidative desulfurization of dibenzothiophene. Fuel, 2016, 174, 9-16.	3.4	86
18	Nitrogen-doped carbon dots with excitation-independent long-wavelength emission produced by a room-temperature reaction. Chemical Communications, 2016, 52, 11912-11914.	2.2	83

#	Article	IF	CITATIONS
19	Biocompatible PEGylated bismuth nanocrystals: "All-in-one―theranostic agent with triple-modal imaging and efficient inÂvivo photothermal ablation of tumors. Biomaterials, 2017, 141, 284-295.	5.7	81
20	Sensitive Room Temperature Photoluminescence-Based Sensing of H ₂ S with Novel CuO–ZnO Nanorods. ACS Applied Materials & Interfaces, 2016, 8, 16379-16385.	4.0	74
21	The polyvinylpyrrolidone functionalized rGO/Bi ₂ S ₃ nanocomposite as a near-infrared light-responsive nanovehicle for chemo-photothermal therapy of cancer. Nanoscale, 2016, 8, 11531-11542.	2.8	71
22	Multifunctional Bi@PPy-PEG Core–Shell Nanohybrids for Dual-Modal Imaging and Photothermal Therapy. ACS Applied Materials & Interfaces, 2018, 10, 1605-1615.	4.0	71
23	Ultrahigh-sensitive optical temperature sensing based on ferroelectric Pr3+-doped (K0.5Na0.5)NbO3. Applied Physics Letters, 2016, 108, .	1.5	69
24	Design and mechanism of core–shell TiO ₂ nanoparticles as a high-performance photothermal agent. Nanoscale, 2017, 9, 16183-16192.	2.8	61
25	Low ost Highâ€Performance Zinc Antimonide Thin Films for Thermoelectric Applications. Advanced Materials, 2012, 24, 1693-1696.	11.1	60
26	Enhanced ethanol sensing properties of ultrathin ZnO nanosheets decorated with CuO nanoparticles. Sensors and Actuators B: Chemical, 2018, 255, 3384-3390.	4.0	55
27	Low-Temperature Solution Synthesis of Black Phosphorus from Red Phosphorus: Crystallization Mechanism and Lithium Ion Battery Applications. Journal of Physical Chemistry Letters, 2020, 11, 2708-2716.	2.1	52
28	Porous Ultrathin NiSe Nanosheet Networks on Nickel Foam for Highâ€Performance Hybrid Supercapacitors. ChemSusChem, 2020, 13, 260-266.	3.6	50
29	Guanine- and Potassium-Based Two-Dimensional Coordination Network Self-Assembled on Au(111). Journal of the American Chemical Society, 2010, 132, 15927-15929.	6.6	49
30	Supramolecular Architectures on Surfaces Formed through Hydrogen Bonding Optimized in Three Dimensions. ACS Nano, 2010, 4, 4097-4109.	7.3	48
31	Gold modified polydopamine coated mesoporous silica nano-structures for synergetic chemo-photothermal effect. Colloids and Surfaces B: Biointerfaces, 2018, 171, 176-185.	2.5	48
32	Upregulation of MiR-205 under hypoxia promotes epithelial–mesenchymal transition by targeting ASPP2. Cell Death and Disease, 2016, 7, e2517-e2517.	2.7	46
33	Supramolecular Porous Network Formed by Molecular Recognition between Chemically Modified Nucleobases Guanine and Cytosine. Angewandte Chemie - International Edition, 2010, 49, 9373-9377.	7.2	45
34	SnSe@SnO ₂ core–shell nanocomposite for synchronous photothermal–photocatalytic production of clean water. Environmental Science: Nano, 2019, 6, 1507-1515.	2.2	45
35	Humanâ€Serumâ€Albuminâ€Coated Prussian Blue Nanoparticles as pHâ€{Thermotriggered Drugâ€Delivery Vehicles for Cancer Thermochemotherapy. Particle and Particle Systems Characterization, 2016, 33, 53-62.	1.2	42
36	Long-range ordered and atomic-scale control of graphene hybridization by photocycloaddition. Nature Chemistry, 2020, 12, 1035-1041.	6.6	41

#	Article	IF	CITATIONS
37	Highly efficient photothermal sterilization of water mediated by Prussian blue nanocages. Environmental Science: Nano, 2018, 5, 1161-1168.	2.2	39
38	The Structure of Atomic Sulfur Phases on Au(111). Journal of Physical Chemistry C, 2007, 111, 10904-10914.	1.5	38
39	Polyethylene glycol-modified cobalt sulfide nanosheets for high-performance photothermal conversion and photoacoustic/magnetic resonance imaging. Nano Research, 2018, 11, 2436-2449.	5.8	36
40	UV photocatalytic activity of Au@ZnO core–shell nanostructure with enhanced UV emission. RSC Advances, 2015, 5, 65595-65599.	1.7	34
41	Interactions of the baicalin and baicalein with bilayer lipid membranes investigated by cyclic voltammetry and UV–Vis spectroscopy. Bioelectrochemistry, 2014, 95, 29-33.	2.4	33
42	Structure Investigation of Ag(111)(â^š7×â^š7)R19°-SCH3by X-ray Standing Waves: A Case of Thiol-Induced Substrate Reconstruction. Journal of Physical Chemistry B, 2006, 110, 2164-2170.	1.2	31
43	From zero to two dimensions: supramolecular nanostructures formed from perylene-3,4,9,10-tetracarboxylic diimide (PTCDI) and Ni on the Au(111) surface through the interplay between hydrogen-bonding and electrostatic metal-organic interactions. Nano Research, 2012, 5, 903-916.	5.8	31
44	Enhanced Multiferroic and Magnetocapacitive Properties of (1Ââ^Â <i>x</i>) <scp><scp>Ba</scp></scp> _{0.7} <scp>Ca</scp> _{0.3} <scp>< Ceramics. Journal of the American Ceramic Society, 2014, 97, 816-825.</scp>	scp 9 TiO<	/sœpo∙
45	STM manipulation of molecular moulds on metal surfaces. Nano Research, 2009, 2, 254-259.	5.8	29
46	Phaseâ€Transition Induced Conversion into a Photothermal Material: Quasiâ€Metallic WO 2.9 Nanorods for Solar Water Evaporation and Anticancer Photothermal Therapy. Angewandte Chemie, 2018, 130, 10826-10831.	1.6	29
47	Scanning Tunneling Microscopy Investigation of the Structure of Methanethiolate on Ag(111). Langmuir, 2005, 21, 7285-7291.	1.6	28
48	Atomic-scale structures and interactions between the guanine quartet and potassium. Chemical Communications, 2013, 49, 7210.	2.2	26
49	Oxidative coupling of anilines to azobenzenes using heterogeneous manganese oxide catalysts. Catalysis Science and Technology, 2016, 6, 1940-1945.	2.1	26
50	Apoptosis-Promoting Effects of Hematoporphyrin Monomethyl Ether-Sonodynamic Therapy (HMME-SDT) on Endometrial Cancer. PLoS ONE, 2015, 10, e0137980.	1.1	26
51	Increasing throughput of AFM-based single cell adhesion measurements through multisubstrate surfaces. Beilstein Journal of Nanotechnology, 2015, 6, 157-166.	1.5	25
52	Incident fluence dependent morphologies, photoluminescence and optical oxygen sensing properties of ZnO nanorods grown by pulsed laser deposition. Journal of Materials Chemistry C, 2015, 3, 2557-2562.	2.7	24
53	White-light-emitting properties of SrTiO ₃ :Pr ³⁺ nanoparticles. RSC Advances, 2015, 5, 27491-27495.	1.7	24
54	Prussian blue-encapsulated Fe3O4 nanoparticles for reusable photothermal sterilization of water. Journal of Colloid and Interface Science, 2019, 540, 354-361	5.0	24

#	Article	IF	CITATIONS
55	Pr ³⁺ -Doped (K _{0.5} Na _{0.5})NbO ₃ as a high response optical oxygen sensing agent. Journal of Materials Chemistry C, 2016, 4, 11508-11513.	2.7	22
56	Core–Shell Bi ₂ Se ₃ @mSiO ₂ â€PEG as a Multifunctional Drugâ€Delivery Nanoplatform for Synergistic Thermoâ€Chemotherapy with Infrared Thermal Imaging of Cancer Cells. Particle and Particle Systems Characterization, 2018, 35, 1700337.	1.2	22
57	Self-assembly of hydrogen-bonded chains of molecular landers. Chemical Communications, 2010, 46, 5545.	2.2	21
58	Diameter-optimized high-order waveguide nanorods for fluorescence enhancement applied in ultrasensitive bioassays. Nanoscale, 2019, 11, 14322-14329.	2.8	21
59	ZnO Nanorod Array Grown on Ag Layer: A Highly Efficient Fluorescence Enhancement Platform. Scientific Reports, 2015, 5, 8152.	1.6	20
60	Xanthine Quartets on Au(111). Journal of the American Chemical Society, 2018, 140, 54-57.	6.6	20
61	Cobalt Phosphide Nanoparticles Applied as a Theranostic Agent for Multimodal Imaging and Anticancer Photothermal Therapy. Particle and Particle Systems Characterization, 2018, 35, 1800127.	1.2	20
62	Identifying the convergent reaction path from predesigned assembled structures: Dissymmetrical dehalogenation of Br2Py on Ag(111). Nano Research, 0, , 1.	5.8	20
63	Rechargeable Mg-Ion Full Battery System with High Capacity and High Rate. ACS Applied Materials & Interfaces, 2021, 13, 40451-40459.	4.0	19
64	Homochiral Xanthine Quintet Networks Self-Assembled on Au(111) Surfaces. ACS Nano, 2011, 5, 6651-6660.	7.3	18
65	In PC3 prostate cancer cells ephrin receptors crosstalk to \hat{I}^21 -integrins to strengthen adhesion to collagen type I. Scientific Reports, 2015, 5, 8206.	1.6	18
66	Mesoporous silica-coated bismuth nanohybrids as a new platform for photoacoustic/computed tomography imaging and synergistic chemophotothermal therapy. Nanomedicine, 2018, 13, 2283-2300.	1.7	18
67	Ultrafast plasmonic lasing from a metal/semiconductor interface. Nanoscale, 2020, 12, 16403-16408.	2.8	18
68	Structural Investigation of the Interaction of Molecular Sulfur with Ag(111). Journal of Physical Chemistry C, 2007, 111, 3152-3162.	1.5	16
69	EGR-1/ASPP1 inter-regulatory loop promotes apoptosis by inhibiting cyto-protective autophagy. Cell Death and Disease, 2017, 8, e2869-e2869.	2.7	14
70	Epigenetic silencing of ASPP1 confers 5â€FU resistance in clear cell renal cell carcinoma by preventing p53 activation. International Journal of Cancer, 2017, 141, 1422-1433.	2.3	14
71	HDAC1-induced epigenetic silencing of ASPP2 promotes cell motility, tumour growth and drug resistance in renal cell carcinoma. Cancer Letters, 2018, 432, 121-131.	3.2	13
72	One-step production of carbon nanocages for supercapacitors and sodium-ion batteries. Journal of Electroanalytical Chemistry, 2020, 878, 114551.	1.9	13

#	Article	IF	CITATIONS
73	Au@SiO2 core/shell nanoparticle-decorated TiO2 nanorod arrays for enhanced photoelectrochemical water splitting. Science Bulletin, 2014, 59, 2191-2198.	1.7	12
74	Hierarchical porous graphitic carbon for high-performance supercapacitors at high temperature. RSC Advances, 2017, 7, 34488-34496.	1.7	12
75	NIR-responsive reversible phase transition of supramolecular hydrogels for tumor treatment. Journal of Materials Chemistry B, 2020, 8, 6429-6437.	2.9	12
76	Onâ€Surface Decarboxylation Coupling Facilitated by Lockâ€toâ€Unlock Variation of Molecules upon the Reaction. Angewandte Chemie - International Edition, 2021, 60, 17435-17439.	7.2	12
77	Formation of Hypoxanthine Tetrad by Reaction with Sodium Chloride: From Planar to Stereo. Angewandte Chemie - International Edition, 2018, 57, 16015-16019.	7.2	11
78	Graphene‣ike Covalent Organic Framework with a Wide Band Gap Synthesized On Surface via Stepwise Reactions. Angewandte Chemie - International Edition, 2020, 59, 15958-15962.	7.2	10
79	Structure of the Pentylthiolate Self-Assembled Monolayer on Ag(111). Journal of Physical Chemistry C, 2007, 111, 10040-10048.	1.5	9
80	Growth and thermoelectric properties of FeSb2 films produced by pulsed laser deposition. Applied Physics A: Materials Science and Processing, 2011, 104, 883-887.	1.1	9
81	Raman study of bromine-doped single-walled carbon nanotubes under high pressure. Journal of Physics Condensed Matter, 2002, 14, 11255-11259.	0.7	8
82	Antibacterial Ag–SiO2 composite films synthesized by pulsed laser deposition. Materials Letters, 2014, 130, 79-82.	1.3	8
83	Subsurfaceâ€Carbonâ€Induced Local Charge of Copper for an Onâ€Surface Displacement Reaction. Angewandte Chemie - International Edition, 2021, 60, 23123-23127.	7.2	6
84	Molecular recognition and homochirality preservation of guanine tetrads in the presence of melamine. Nano Research, 2020, 13, 2427-2430.	5.8	5
85	Formation of Hypoxanthine Tetrad by Reaction with Sodium Chloride: From Planar to Stereo. Angewandte Chemie, 2018, 130, 16247-16251.	1.6	4
86	Inhibition of Lysozyme Fibrillation by Gold Nanorods and Nanoparticles. Journal of Nanoscience and Nanotechnology, 2018, 18, 3087-3094.	0.9	4
87	Au@MnSe ₂ Core–Shell Nanoagent Enabling Immediate Generation of Hydroxyl Radicals and Simultaneous Glutathione Deletion Free of Preâ€Reaction for Chemodynamicâ€Photothermoâ€Photocatalytic Therapy with Significant Immune Response. Advanced Healthcare Materials. 2022. 11. e2200041.	3.9	4
88	An efficient dual functional Raman and Fluorescence detection platform achieved by controlling the electromagnetic enhanced field in three-dimensional Ag/ZnO composited arrays. Materials Advances, 2022, 3, 4520-4525.	2.6	3
89	Aqueous Nickel-Ion Batteries with Long Lifetime, High Capacity, and High Rate Capability Based on K ₂ V ₆ O ₁₆ A·1.64H ₂ O Cathodes. Energy & Fuels, 0, , .	2.5	3
90	On‣urface Decarboxylation Coupling Facilitated by Lockâ€ŧoâ€Unlock Variation of Molecules upon the Reaction. Angewandte Chemie, 2021, 133, 17575-17579.	1.6	2

		Μιαο Υυ		
#	Article		IF	CITATIONS
91	Fabrication of Co0.85Se@CN double-walled hollow cages to address the volume expar and enhance ion diffusion for sodium-ion storage. Electrochimica Acta, 2022, 426, 140	ision of anode 1839.	2.6	2
92	Three-dimensional hydrogen bonding between Landers and planar molecules facilitated electrostatic interactions with Ni adatoms. Chemical Communications, 2018, 54, 8845	l by -8848.	2.2	1
93	Grapheneâ€Like Covalent Organic Framework with a Wide Band Gap Synthesized On S Reactions. Angewandte Chemie, 2020, 132, 16092-16096.	Surface via Stepwise	1.6	1
94	Superâ€robust Xanthineâ€Sodium Complexes on Au(111). Angewandte Chemie - Inter	national Edition, 2022, , .	7.2	1
95	Subsurfaceâ€Carbonâ€Induced Local Charge of Copper for an Onâ€Surface Displacem Angewandte Chemie, 2021, 133, 23307.	ent Reaction.	1.6	Ο
96	Superâ€robust Xanthineâ€Sodium Complexes on Au(111). Angewandte Chemie, 0, , .		1.6	0